International Journal of Imaging Systems and Technology, Vol. 23, Issue 3, 235–248 (2013)

Brain MRI Denoizing and Segmentation Based on Improved Adaptive Nonlocal Means

Muhammad Aksam Iftikhar,* Abdul Jalil, Saima Rathore, Ahmad Ali, Mutawarra Hussain

Department of Computer and Information Sciences, Pakistan Institute of Engineering and Applied Sciences, Islamabad, Pakistan

Received 8 February 2013; revised 26 March 2013; accepted 19 April 2013

ABSTRACT: Denoizing of magnetic resonance (MR) brain images has been focus of numerous studies in the past. The performance of subsequent stages of image processing, in automated image analysis, is substantially improved by explicit consideration of noise. Nonlocal means (NLM) is a popular denoizing method which exploits usual redundancy present in an image to restore noise free image. It computes restored value of a pixel as weighted average of candidate pixels in a search window. In this article, we propose an improved version of the NLM algorithm which is modified in two ways. First, a robust threshold criterion is introduced, which helps selecting suitable pixels for participation in the restoration process. Second, the search window size is made adaptive using a window adaptation test based on the proposed threshold criterion. The modified NLM algorithm is named as improved adaptive nonlocal means (IANLM). An alternate implementation of IANLM is also proposed which exploits the image smoothness property to yield better denoizing performance. The computational burden is reduced significantly due to proposed modifications. Experiments are performed on simulated and real brain MR images at various noise levels. Results indicate that the proposed algorithm produces not only better denoizing results (quantitatively and qualitatively), but is also computationally more efficient. Moreover, the proposed technique is incorporated in an already proposed segmentation framework to check its validity in the practical scenario of segmentation. Improved segmentation results (quantitative and qualitative) verify the practical usefulness of the proposed algorithm in real world medical applications. Int J Imaging Syst Technol, 23, 235–248, 2013; Published online in Wiley Online Library (wileyonlinelibrary.com). DOI: 10.1002/ima.22057

Key words: nonlocal means; adaptive; denoizing; brain MRI; segmentation

I. INTRODUCTION

Brain MR Image analysis is a common medical practice to diagnose various brain diseases such as tumor, multiple sclerosis, Alzhiemer's disease, and so on. The study of different brain tissues, such as cerebrospinal fluid (CSF), gray matter (GM), and white matter (WM), is central to computer-aided diagnosis and analysis. The brain MR images are processed in several stages during such computer-aided analysis. However, the images acquired by MR imaging equipment may undergo different types of degradations which hinder the subsequent processing stages. These degradations may be caused by several factors such as operator error and limitations imposed by the imaging equipment. Noise is a common degradation, which significantly deteriorates the MR image quality. This inherent noise should be removed for effective results prior to subsequent image processing stages.

The type of noise present in MR images is usually Rician (Gudbjartsson et al., 1995; Macovski, 1996), which is known to be difficult to remove as compared to other types of noise (Coupe et al., 2008). Various techniques have been applied to attack the problem of noise including anisotropic diffusion (Gerig et al., 1992), wavelet-based techniques (Nowak, 1999), and others (Bankman, 2000). Among these techniques, NLM (Buades et al., 2005) has drawn the interest of many researchers due to its superior denoizing and detail preservation characteristics. It is a nonlocal neighborhood averaging algorithm, based on weighted average of pixels within a large search window. The term nonlocal is attributed to the larger size search window as compared to smaller window size of traditional local neighborhood based approaches. The NLM algorithm is not only effective in removing noise from image but also preserves fine image details. It is similar in approach to Yaroslavsky (1985) work which involves gray level similarity computation between a noisy pixel and its neighbors rather than spatial similarity. However, NLM employs similarity between neighboring windows of pixels (called patches) instead of pixels themselves. This idea of patch comparison is inspired by Discrete Universal Denoizing (DUDE) algorithm (Ordentlich et al., 2003). Images in practice usually contain much redundancy in their local structures. Because of such redundancy, the patch of a noisy pixel is expected to be close to the patch of another pixel in a search area. Hence, the pixel of interest can be restored by weighted averaging of pixels with similar patches.

Several modifications have been made to the classical NLM algorithm to improve its denoizing performance and computational

Correspondence to: Muhammad Aksam Iftikhar;
e-mail: aksam.iftikhar@gmail.com

Grant sponsor: PIEAS-administered Endowment Fund (provided by Higher Education Commission Pakistan, for Higher eductation and R&D in IT and Telecom Sector).

efficiency. Yan et al. (2012) improved the denoizing performance of NLM by increasing the number of suitable candidate pixels to be included in restoring the value of a particular pixel. Their work was based on a preprocessing step of classifying the pixels in input image into similar clusters. The method in Liu et al. (2008) presents a robust and fast variant of NLM that incorporates the concept of Laplacian pyramid into classical NLM.

A substantial contemporary literature deals with brain MRI denoizing. In Manjon et al. (2008), authors applied NLM to brain MR images to obtain optimal parameters of the algorithm. In Aksam et al. (2012), parameters optimization for brain MRI denoizing using NLM has been achieved by employing Genetic Algorithm. In Coupe et al. (2008), authors presented a fast and effective method for 3D brain MRI denoizing based on voxel pre-selection and a block-wise implementation. The work of Vega et al. (2012) is based on comparing features of patches instead of their intensities. This salient feature matching approach leads to fast and improved denoizing, as verified by brain MR data denoizing, achieved by using this method. In Gal et al. (2010), authors proposed dynamic NLM algorithm adopted to the special nature of dynamic contrast-enhanced (DCE) magnetic resonance images. Spatially varying noise level is handled in Manjon et al. (2010), where authors introduced an adaptive nonlocal means algorithm, taking into account the local noise level. Some authors have also studied the effect of the search window size of the NLM algorithm (Salmon, 2010; Thaipanich et al., 2010). In Salmon (2010), the two parameters of the NLM algorithm, namely the search window size and central patch weight, have been studied. In Thaipanich et al. (2010), the search window size is made adaptive for different region types in the image. This work is similar to the one presented in this article, in the sense that search window size is made adaptive. However, our approach considers a robust threshold criterion based adaptive search window, which is independent of the region type. The implementation of our proposed algorithm is also novel and complementary to the proposed approach (see Section III).

Image segmentation is usually a subsequent processing step in an automated image analysis application. It has found several application in the field of medical imaging (Kwon et al., 2003; Saha et al., 2011; Hassan et al. 2012). Robust MR image segmentation can be obtained by embedding the nonlocal information into fuzzy segmentation framework. In Zhao et al. (2011), for example, a nonlocal spatial constraint term is added to the objective function of classical fuzzy c-means clustering. Similarly, a weighted image patch-based FCM is proposed in Ji et al. (2012) which replaces image pixels with patches and constructs a weighing scheme in the clustering process based on these patches. Another nonlocal fuzzy c-means algorithm is proposed specifically for details preservation in synthetic aperture radar (SAR) images (Feng et al., 2013). In this approach, a new image is generated which is more robust to multiplicative speckle noise present in MR images. The new image is generated based on nonlocal information and rectified edge parts are located using coefficient of variation and orientation based statistics. The nonlocal framework embedded in above approaches enhances to a great extent their robustness to noise.

In this article, we present an improved variant of the classical NLM algorithm. The improvement is two-fold. First, while denoizing a particular pixel, we consider only those pixels in its neighborhood which have similarity weights greater than a particular threshold—the so-called robust threshold criterion. Second, the search window size is made adaptive for each pixel. To better exploit the image smoothness property, an alternate traversal mechanism of the search window is proposed instead of conventional row/column wise traversal. These modifications to the classical NLM algorithm give rise to Improved Adaptive NLM (IANLM), which is not only more robust to noise, but is also computationally more efficient. The proposed algorithm is also used in a segmentation framework presented in Zhao et al. (2011), which served to verify the practical applicability of the algorithm in real world applications. The results of denoizing and segmentation, compared to classical NLM, verify the effectiveness and efficiency of IANLM.

The remainder of this article is organized as follows. Section II describes the NLM algorithm and introduces a few notations to be used in the text. Section III presents the proposed scheme and its novel implementation. Comparative results of different denoizing schemes, applied to simulated and real brain MR images, are presented in Section IV. Practical usefulness of the proposed scheme is validated in Section V by integrating it into a segmentation framework. Finally, Section VI concludes the article. Various abbreviations have been used throughout the text to refer to different terms. Table I describes these abbreviations and corresponding terms for reference purpose. In our denoizing and segmentation experiments, simulated brain MR images are corrupted by Rician noise of various levels (percentages). However, signal-to-noise ratio (SNR) is a convenient way of specifying the amount of noise in an image. Therefore, we also relate noise percentage to average SNR for simulated brain MR images in Table II.

II. PRELIMINARIES

A. Notations. The NLM algorithm involves different elements and parameters. It is useful to set up a nomenclature for these elements which may be used consistently throughout the text. We introduce the following notations to formally describe different elements in NLM procedure. **Note the bold-face notation to identify a vector.**

Ω_2	The input image, in 2D space, of size MxN.
y_i	Intensity value observed at input image pixel i.
x_i	Intensity value restored by NLM filter for pixel i.
x_i'	Intensity value restored by IANLM filter for pixel i.
s	Radius of the search window.
$\boldsymbol{S_i}$	Set of pixels belonging to search window around pixel i, where $\lvert S_i \rvert = (2s+1)^2$.
p	Radius of an image patch.
$\boldsymbol{P_i}$	Set of pixels belonging to patch of pixel i, where $\lvert P_i \rvert = (2p+1)^2$.
$\boldsymbol{y(P_i)}$	Intensity values observed at each pixel in P_i i.e. $y(P_i) = (y^{(1)}(P_i), y^{(1)}(P_i),\ldots,y^{(\lvert P_i \rvert)}(P_i))$.
h	Smoothing parameter; controls tradeoff between edge preservation and noise removal.
k	Scaling parameter; used to scale the smoothing parameter for a particular application.
σ	Sigma; the standard deviation of noise
w_{ij}	Similarity weight between pixel i and j, used when restoring the value of pixel i.
w_θ	Threshold value used in robust threshold criterion of IANLM.
N_f	Desired number of pixels(patches) satisfying the threshold criterion.

B. NLM Filter. The denoizing in NLM algorithm relies on a weight function that computes similarity between neighboring windows of noisy pixels. For each pixel i in the image, its local neighborhood (patch) is compared with that of every pixel j in a search window of size $\lvert \boldsymbol{S_i} \rvert$ (radius s). The local neighborhood of pixel i is referred as patch ($\boldsymbol{P_i}$) of pixel i throughout the following text. This

Table I. Abbreviations used in the text.

Abbreviation	Text
MRI	Magnetic resonance imaging
WM	White matter
GM	Gray matter
CSF	Cerebrospinal fluid
DCE	Dynamic contrast enhanced
NLM	Non-local means
IANLM	Improved adaptive non-local means
PSNR	Peak signal to noise ratio
RMSE	Root mean square error
FE	Function evaluations
SA	Segmentation accuracy
DC	Dice coefficient
FCM	Fuzzy c-means
SFCM	Spatial fuzzy c-means
FLICM	Fuzzy local information c-means
FCM_NLS	Fuzzy c-means with non-local spatial information
FCM_INLS	Fuzzy c-means with improved non-local spatial information

similarity comparison, between two patches $\boldsymbol{P_i}$ and $\boldsymbol{P_j}$, is made in terms of Euclidean distance of corresponding intensity values in patches which has been proven to be reliable enough as a distance measure (Coupe et al., 2008). The similarity is measured by a weight term, expressed in the following equation.

$$w_{ij} = \frac{1}{Z_i} e^{-\frac{\left(\|y(\boldsymbol{P_i}) - y(\boldsymbol{P_j})\|_2^2\right)}{h^2}} \tag{1}$$

where $y(\boldsymbol{P_i})$ and $y(\boldsymbol{P_j})$ represent intensity values observed at pixels contained within patch $\boldsymbol{P_i}$ and $\boldsymbol{P_j}$, respectively. The factor h is a tradeoff parameter that controls balance between the noise removal and detail preserving capabilities of the algorithm. Higher the value of h, more noise will be removed. However, a too high value may introduce undesirable blurring. Similarly, a very low value may not be able to remove noise completely and leave undesirable artifacts in the image. Hence, this parameter is related to the amount of noise in the image and is normally used with a scaling parameter, that is, $h = k\sigma$, where σ is the noise level. According to NLM, the restored value x_i of pixel i is computed as in following equation.

$$x_i = \sum_{j \in S_i} w_{ij} y_j \quad \text{subject to} \quad \sum_{j \in S_i} w_{ij} = 1 \quad \text{and} \quad w_{ij} \in [0, 1] \tag{2}$$

where S_i is a search window around pixel i and x_i is the NLM-restored value for pixel i. The two constraints specify that weight w_{ij} lies between 0 and 1 and the sum of weights over a particular window equals 1. The constraints are satisfied due to the normalization factor Z_i in Eq. (1), computed as follows.

$$Z_i = \sum_{j \in S_i} e^{-\frac{\left(\|y(\boldsymbol{P_i}) - y(\boldsymbol{P_j})\|_2^2\right)}{h^2}} \tag{3}$$

Table II. Performance comparison in terms of PSNR.

Noise %	1	2	3	4	5	6	7	8	9
SNR	31.11	27.33	25.78	21.53	19.08	17.52	16.06	14.95	13.82

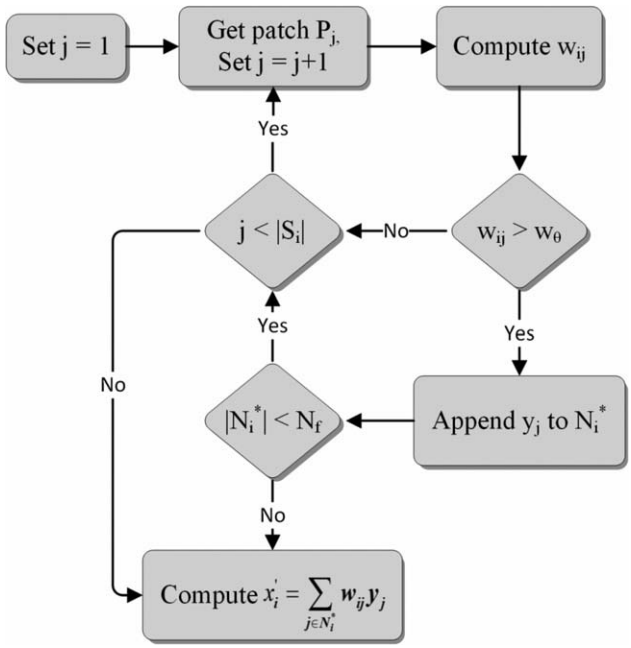

Figure 1. Graphical illustration of restoration process of pixel *i*in IANLM.

III. PROPOSED SCHEME

The conventional NLM algorithm involves a few parameters which need to be tuned for a particular application. The search window size s is an important parameter which is critical both in terms of denoizing performance and computational efficiency. Larger value of s may increase the performance, as more similar patches can be found in a larger search area. However, a window size greater than a certain value may stop yielding better performance (Salmon, 2010). Conversely, the larger the window size more will be the computational burden. Hence, a suitable window size is always desirable for better denoizing. In this section, we propose a variant of conventional NLM, named as improved adaptive nonlocal means (IANLM), by making the search window size adaptive based on a robust threshold criterion.

A. Improved Adaptive Nonlocal Means Denoizing. We have proposed two valuable modifications to the conventional NLM algorithm. First, pixel j, in neighborhood of pixel i, participate in the restoration process of pixel i, only if it satisfies a robust threshold criterion. The criterion states that a pixel (patch) j is considered only if weight $w_{ij} > w_\theta$, where w_θ is a weight threshold. We call the pixel (patch), which satisfies the threshold criterion, as the *fit* pixel (patch). Second, the window size is made adaptive based on this threshold criterion. In particular, the process of patch comparison is terminated as soon as we have N_f fit pixels (patches) available within current search window which satisfy the robust threshold criterion. Hence, both the modifications are complementary to each other. Restoration of a particular pixel in IANLM is shown, graphically, in Figure 1.

Mathematically, the process of denoizing in IANML is formulated slightly different from NLM, and is given in Eq. (4).

$$x_i' = \sum_{j \in N_i^*} w_{ij} y_j \quad \text{subject to} \quad \sum_{j \in N_i^*} w_{ij} = 1 \quad \text{and} \quad w_{ij} \in [0, 1] \tag{4}$$

where x_i' is the IANLM-restored value for pixel i and $N_i^* \subseteq S_i$ is the set of pixels around pixel i, satisfying following constraints.

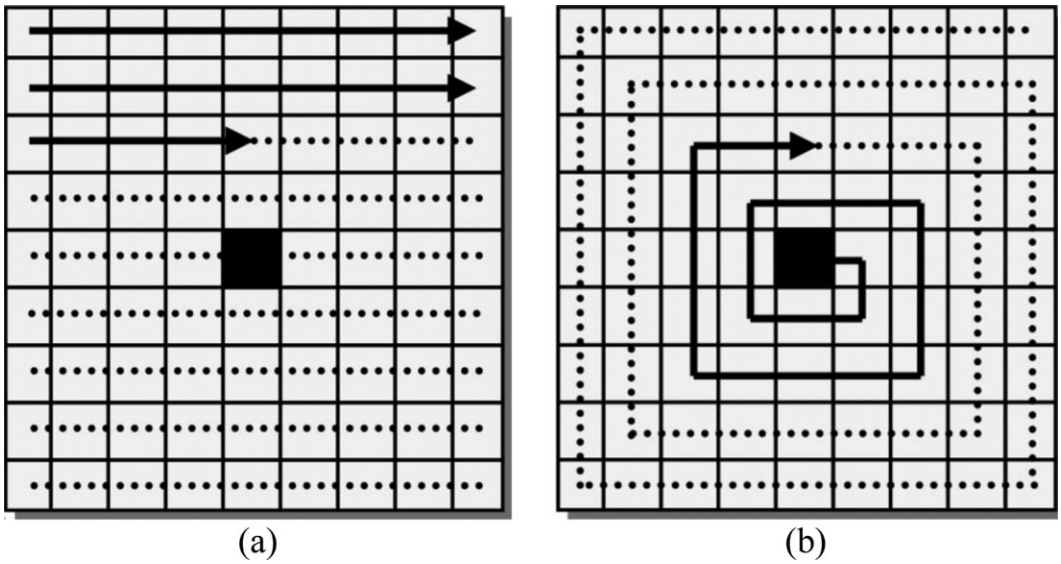

Figure 2. Different window traversal mechanisms (a) Conventional traversal, (b) Spiral traversal.

- Robust threshold criterion: $w_{ij} > w_\theta$, where w_θ is the weight threshold and related to the amount of noise present in the image.
- Window adaptation test: $|N_i^*| \leq N_f$, where N_f is the desired number of fit patches which satisfy the robust threshold criterion and is application dependent.

The algorithm introduces two new parameters i.e. w_θ and N_f, while relaxing the search window size parameter of conventional NLM. Search window size is treated in IANLM as the maximum search window size, that is, the maximum size of window that should be searched adaptively. The parameter w_θ is related to the amount of noise in the image and can be set empirically or as a function of noise level in the image. The suitable value of the parameter N_f is application specific. However, as we will see in Section IV.C.1, the proposed technique is not much sensitive to this parameter if we assign it a sufficiently high value.

B. Proposed Algorithm Implementation. In conventional NLM, the search window is traversed row/column wise to find similar patches. This process is shown graphically in Figure 2a for a 9 × 9 window. The order of search is immaterial in NLM, as complete window search is performed irrespective of the order. However, in IANLM, the window adaptation test ensures that only first N_f pixels are considered within a search window which satisfy the threshold criterion. We propose an alternate search window traversal mechanism based on region growing which exploits this fact positively. The traversal is started from central pixel, and while moving outwards, a spiral path is followed. The process of traversal is terminated as soon as N_f patches are available within the search window. Because of the image regularity/smoothness assumption, it is expected to find more similar patches near the central pixel rather than far away, as in conventional traversal mechanism. Thus, the alternate region growing based search window traversal exploits local information better in the denoizing process. This also improves the computational efficiency of IANLM as desired number of patches N_f are found earlier than in conventional traversal. The boundary pixels, where only partial neighborhoods are available for comparison, are handled by zero padding on image borders. Figure 2b shows an example of a 9 × 9 window, traversed using spiral traversal mechanism.

The alternate spiral traversal is efficiently implemented in pseudo codes, presented in Figures 3 and 4, which cause no significant overhead for spiral implementation. The first pseudo code employs a spiral index window, equal in size to that of the search window, which specifies the order in which patch comparisons should be made in the proposed traversal mechanism. A spiral window for $R = 5$, for example, is shown in Figure 5a, where $R = 2s + 1$. Popular computational tools, like MATLAB, can generate such spiral window as a built-in feature. The output of first pseudo code is a coordinates offset vector (window), sorted in spiral order for each pixel in the search window, relative to the central pixel. The offset vector is generated using the spiral window generated earlier. An offset window, generated using spiral window in Figure 5a, is shown in Figure 5b. Note that the first pseudo code is executed only once to generate the offset vector. The second pseudo code simply uses the offset vector for each search window in

Pseudo Code-I (Generate offset vector)

1. Input: pixel i (the window central pixel), $j \in N_i$.
2. Let $R = (2s+1)$, where s is search window size (radius).
3. Generate a square spiral window, $SpWin$ = Spiral(R).
4. Generate an offset window as follows.
   a. ind = sort($SpWin$); indices of sorted values in $SpWin$ are returned in ind.
   b. [i,j]=ToCoordinates(ind); get coordinates corresponding to ind.
   c. $offset$ = [i j]-((R+1)/2); compute coordinates offsets for each location in window.
5. $offset$ contains offsets corresponding to spiral traversal.

Figure 3. Pseudo code for generating offset vector.

```
Pseudo Code-II (Traverse the window)
1. Input: let s, t be coordinates of central pixel of an RxR window
2. for i = 1 to R^2
3.         (p,q) ← offset(i); get coordinates offsets corresponding to i_th element in offset
4.         u = s + p;
5.         v = t + q; generate coordinates of next pixel
6.         j ← ToIndex(u, v) ; convert coordinates (u, v) to image index j.
7.         IANLM(j) ; perform IANLM for pixel j.
8. end for
```

Figure 4. Pseudo code for spiral traversal of the window.

the image and computes the coordinates of next pixel, to be processed, in the proposed spiral traversal. Once, the next pixel is obtained, it is processed using IANLM as described in Section III.A.

IV. RESULTS AND DISCUSSIONS

The proposed modified NLM algorithm is extensively studied in the following experiments and the performance is validated both quantitatively and qualitatively. Both simulated and real brain MR images are denoized using NLM and the proposed technique under different parameter settings. Denoizing performance of different variants of IANLM is compared with conventional NLM in terms of well-known performance metrics (see Section IV.B). To be more precise, the proposed spiral traversal of IANLM is implemented in addition to the traditional row/column wise traversal and the two parameters of the proposed algorithm are studied in different variants for application to brain MR images.

The first parameter of the proposed technique, named as w_θ, is related to the amount of noise present in the image. Therefore, this parameter has been studied as a function of the noise level, as well as a fixed empirical value of the parameter is also tested. The second parameter, named as N_f, is selected empirically by comparing the performance of proposed algorithm at different noise levels. To put things together, performance measures are obtained for the following algorithm settings.

- The conventional NLM
- The proposed IANLM algorithm employing conventional window traversal (IANLM-0)
- The proposed IANLM algorithm employing spiral window traversal by using

  w_θ as function of noise level (IANLM-1, IANLM-2)
  w_θ fixed empirically (IANLM-3)

All the experiments were performed on a core i7 workstation with 3.40 GHz CPU and 16 GB RAM. However, only one core was utilized during processing, as no parallel code is implemented. The computational tool used for our experiments is MATLAB R2011b (7.13.0.564).

A. Data sets. The denoizing experiments have been conducted with real and simulated brain MR images. Synthetic normal brain MR images have been obtained from publicly available Simulated Brain Database (SBD), named as BrainWeb (Collins et al., 1998). BrainWeb is a standard simulated MRI data set for brain segmentation. The simulated images have been generated using an MRI simulator (Kwan et al., 1996), developed at the McConnell Brain Imaging Centre. The slice thickness value used for the BrainWeb database is 1 mm and scan type is T_1-weighted. From the 3D T_1-weighted simulated brain volume of size 181 × 217 × 181, we have performed experiments on 25 consecutive 2D slices, where maximum of the brain volume is visible. The experimental results have been summarized by averaging the results over these brain MR images.

Real brain MR data consists of 3D brain MR volume publicly available from the Open Access Series of Imaging Studies (OASIS, www.oasis-brains.org) database (Marcus et al., 2007). This database contains structural MRI scans of various subjects which are aimed at assessing the reproducibility of segmentation techniques. However, we have used the data set to measure the effectiveness of our proposed technique to remove inherent noise in these MR images. The brain MR data from this data set, which we used in our experiments, is a T_1-weighted 3D magnetic resonance imaging volume of subject 111 from OASIS database. The size of data set is 180 × 256 × 256 and slice thickness is 1.25 mm. The denoizing experiments are performed on the said data set and qualitative denoizing results are obtained.

B. Performance Metrics. The performance of denoizing brain MR images using NLM and different variations of the proposed technique is measured on two aspects. First, the denoizing capability is measured in terms of three well-known metrics, that is, Root Mean

21	22	23	24	25
20	7	8	9	10
19	6	1	2	11
18	5	4	3	12
17	16	15	14	13

(a)

-2, -2	-2,-1	-2,0	-2,1	-2,2
-1, -2	-1,-1	-1,0	-1,1	-1,2
0, -2	0,-1	0,0	0,1	0,2
1, -2	1,-1	1,0	1,1	1,2
2,-2	2,-1	2,0	2,1	2,2

(b)

Figure 5. (a) Spiral window ($R = 5$), and corresponding (b) Offset window.

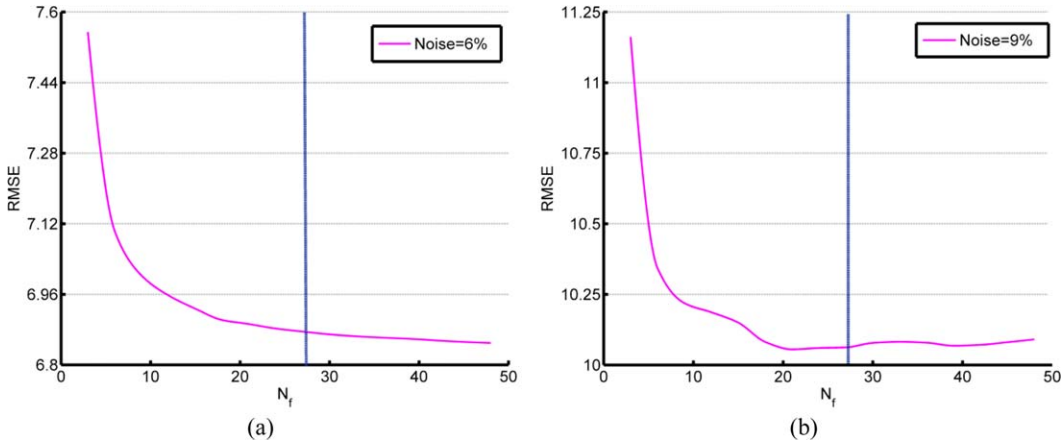

Figure 6. Selection of optimal value for N_f using average RMSE for IANLM-filtered images originally corrupted with (a) 6% noise, (b) 9% noise. [Color figure can be viewed in the online issue, which is available at wileyonlinelibrary.com.]

Square Error (RMSE), Peak Signal to Noise Ratio (PSNR) and correlation coefficient. RMSE reflects how much results of an experiment deviate from the expected value. It is calculated as follows.

$$\mathrm{RMSE} = \sqrt{\frac{1}{M \times N} \sum_{m=1}^{M} \sum_{n=1}^{N} [I_1(m,n) - I_2(m,n)]^2} \qquad (5)$$

where, in context of denoizing, I_1 and I_2 represent original and restored images, respectively. The factors M and N represent the height and width of the image, respectively.

PSNR is the ratio between the maximum possible power of a signal and power of noise level that corrupts the signal. PSNR and RMSE are related by the following equation.

$$\mathrm{PSNR} = 10 \log_{10}\left(R^2/\mathrm{MSE}\right) = 20 \log_{10}(R/\mathrm{RMSE}) \qquad (6)$$

where R is the maximum possible pixel intensity value in the image and RMSE is the same as in Eq. (5).

The correlation coefficient is also referred simply as correlation. The correlation between two data sets is high when the data sets are strongly linked together. It is computed using following expression.

$$\mathrm{Correlation} = \sum_{i=1}^{n} (x_i - \bar{x})(y_i - \bar{y}) / \sum_{i=1}^{n} (x_i - \bar{x})^2 \sum_{i=1}^{n} (y_i - \bar{y})^2 \qquad (7)$$

where x_i and y_i refer to the elements of data sets x and y and n is the size of each data set. Moreover, $\bar{x}$ and $\bar{y}$ represent the mean values of data sets x and y, respectively. In our case, the data sets are the images to be compared.

The second aspect of the performance measures reveals the computational advantage of the proposed algorithm over classical NLM. The computational complexity of different denoizing algorithms, used in experiments, is measured in terms of number of function evaluations (FE) and CPU time taken to run the algorithm. In the NLM algorithm (and the proposed variant), the most (computationally) expensive task is to compare patches for computing similarity weights. Hence, we have used number of patch comparisons as number of function evaluations for each algorithm. The CPU time is measured in number of seconds and simply equals the average time, taken by an algorithm, to denoize the input image at a particular noise level.

C. Experiments with Simulated Images. In this section, we validate the performance as well as computational efficiency of the proposed scheme. The conventional NLM and different variants of IANLM (IANLM-0, IANLM-1, IANLM-2, IANLM-3) are applied to simulated brain MR image denoizing, corrupted by Rician noise at different levels. The optimal values of different parameters of the nonlocal framework for brain MRI denoizing have been proposed in contemporary literature (Manjon, et al., 2008). We have performed extensive experimentation and found that the proposed values are reasonable for a general framework of brain MRI denoizing. Hence, we use $s = 5$, $p = 2$, and $h = 1.2\sigma$ for subsequent experiments.

The variant IANLM-0 implements the conventional row/column wise search window traversal, while others implement the proposed spiral traversal. Moreover, these variants test the effect of w_θ which is another important parameter of the proposed algorithm. IANLM-3 fixes $w_\theta = 0.01$, which is empirically found to be suitable for denoizing at all noise levels. The other two variants, IANLM-1 and IANLM-2, exploit the relationship of w_θ to the amount of noise in the image. Generally, at lower noise level, a higher value of w_θ is desired to obtain enough patches with sufficient similarity and vice versa. Therefore, IANLM-1 and IANLM-2 use $w_\theta = 1/\sigma^2$ and $w_\theta = 1/\sigma$, respectively, where σ is the level (standard deviation) of noise in the image. These two variants relax the requirement to set w_θ empirically, which may be undesirable in some medical applications.

C.1. Parameter Selection. An important parameter of the proposed IANLM algorithm, the number of fit patches (N_f), is set empirically, prior to obtaining results at different noise levels for IANML0–3. The simulated brain MR images, corrupted by higher noise levels (6 and 9%), are denoized using the proposed technique for different values of N_f. The empirical selection of N_f is shown in Figure 6 where average RMSE values are plotted against N_f. We observe from Figures 6a and 6b, that after $N_f \approx 27$, RMSE values come to a much steady state and increasing N_f beyond this point does not yield better results. Therefore, we have used an empirical value of $N_f = 27$ in subsequent experiments. It is worth to be noted that behavior of RMSE against N_f is almost similar for all variants of

Table III. Performance comparison in terms of PSNR.

Noise (%)	PSNR				
	NLM	IANLM-0	IANLM-1	IANLM-2	IANLM-3
1	38.66 ± 0.05	44.11 ± 0.04	43.29 ± 0.04	43.18 ± 0.04	43.88 ± 0.04
2	36.96 ± 0.06	38.99 ± 0.05	38.78 ± 0.04	38.32 ± 0.04	39.36 ± 0.04
3	35.32 ± 0.05	36.33 ± 0.05	36.26 ± 0.04	35.55 ± 0.05	36.57 ± 0.05
4	33.72 ± 0.05	34.37 ± 0.05	34.38 ± 0.05	33.76 ± 0.05	34.47 ± 0.05
5	32.26 ± 0.05	32.68 ± 0.04	32.77 ± 0.05	32.38 ± 0.05	32.77 ± 0.05
6	30.95 ± 0.05	31.17 ± 0.05	31.36 ± 0.05	31.17 ± 0.05	31.34 ± 0.04
7	29.79 ± 0.05	29.76 ± 0.05	30.11 ± 0.05	30.06 ± 0.05	30.09 ± 0.05
8	28.75 ± 0.05	28.49 ± 0.05	29.06 ± 0.05	29.07 ± 0.05	29.04 ± 0.05
9	27.81 ± 0.05	27.36 ± 0.05	28.08 ± 0.05	28.10 ± 0.04	28.08 ± 0.05

Table IV. Performance comparison in terms of RMSE.

Noise (%)	RMSE				
	NLM	IANLM-0	IANLM-1	IANLM-2	IANLM-3
1	2.98 ± 0.02	1.59 ± 0.01	1.75 ± 0.01	1.77 ± 0.01	1.63 ± 0.01
2	3.62 ± 0.02	2.87 ± 0.01	2.94 ± 0.01	3.10 ± 0.01	2.75 ± 0.01
3	4.37 ± 0.03	3.89 ± 0.02	3.92 ± 0.02	4.26 ± 0.02	3.79 ± 0.02
4	5.26 ± 0.03	4.88 ± 0.03	4.87 ± 0.03	5.23 ± 0.03	4.82 ± 0.03
5	6.22 ± 0.04	5.92 ± 0.03	5.86 ± 0.03	6.13 ± 0.03	5.86 ± 0.03
6	7.23 ± 0.04	7.05 ± 0.04	6.90 ± 0.04	7.04 ± 0.04	6.91 ± 0.03
7	8.26 ± 0.04	8.29 ± 0.04	7.96 ± 0.04	8.01 ± 0.05	7.99 ± 0.05
8	9.31 ± 0.06	9.60 ± 0.06	8.99 ± 0.05	8.98 ± 0.05	9.01 ± 0.05
9	10.38 ± 0.05	10.93 ± 0.06	10.06 ± 0.05	10.04 ± 0.05	10.07 ± 0.05

IANLM. However, for simplicity, results are shown only for IANLM-1 in Figure 6.

C.2. Performance Analysis. In this section, we denoize simulated brain MRI data, corrupted by various noise levels, using NLM, IANLM-0, IANLM-1, IANLM-2, and IANLM-3. The performance measures are obtained in terms of PSNR, RMSE and correlation at nine different noise levels. The denoizing process is carried out 20 times by adding certain amount of noise to each image slice and average results, over all slices, are presented in Tables III and IV and Figure 7 for each noise level.

Quantitative results in Tables III and IV show superiority of IANLM algorithm over conventional NLM at all noise levels. The proposed implementation of the algorithm also outperforms the conventional implementation (IANLM-0) with exception of a few lower noise levels. Conventional traversal based scheme IANLM-0 performs poorly at higher noise levels as compared to spiral traversal based IANLM schemes. Similar conclusion is drawn from the results obtained in terms of correlation measure, which are shown graphically in Figure 7. The performance of IANLM-1 and IANLM-3 surpasses other techniques at all noise levels in terms of correlation

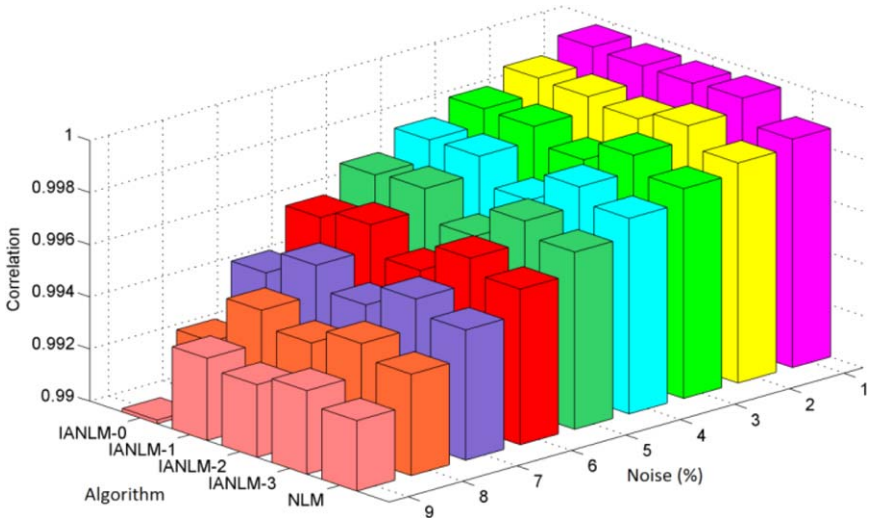

Figure 7. Performance comparison in terms of Correlation measure. [Color figure can be viewed in the online issue, which is available at wileyonlinelibrary.com.]

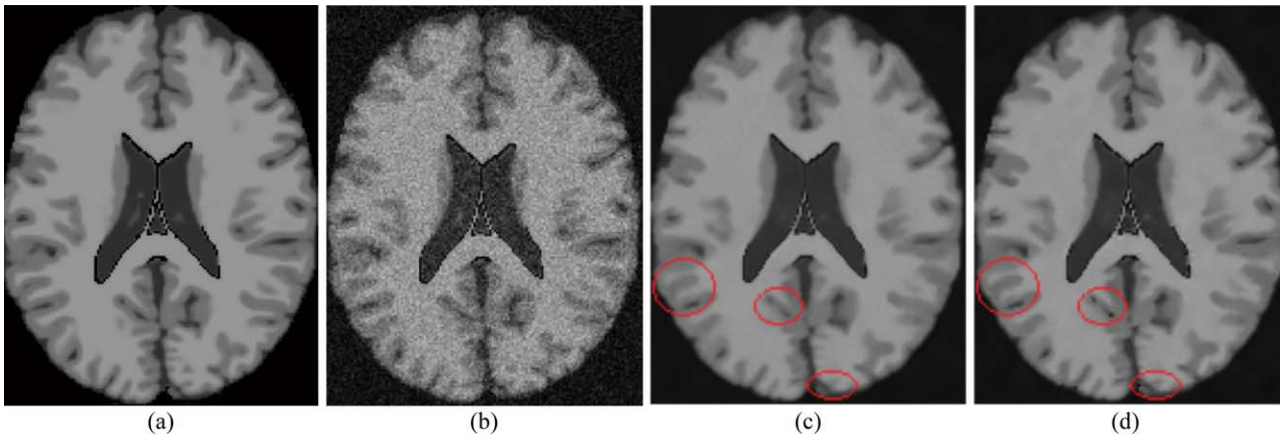

Figure 8. Qualitative comparison of denoizing results (a) original image, (b) noisy image (9% noise), (c) NLM-filtered image (d) IANLM-filtered Image. [Color figure can be viewed in the online issue, which is available at wileyonlinelibrary.com.]

measure. However, conventional traversal based IANLM-0 performs poorly at higher noise levels.

Among three spiral traversal based variants of IANLM, we recommend IANLM-1 for two reasons. First, the performance of IANLM-1 is superior as compared to IANLM-2 at almost all noise levels. Second, IANLM-1 is preferable over IANLM-3, as it eliminates the need to empirically adjust the value of w_θ. Therefore, we will be using IANLM-1 to demonstrate the results of subsequent experiments and it will be called simply as IANLM.

Figure 8 qualitatively compares the results of applying NLM and the proposed IANLM to a particular slice from the 3D BrainWeb image database. The original and noisy slice images (9% noise) are shown in Figures 8a and 8b, respectively. Corresponding images, restored by NLM and the proposed IANLM, are shown in Figures 8c and 8d. It can be observed by visual inspection that the restored image produced by IANLM is sharper as compared to NLM. Moreover, the proposed technique is able to preserve small structures more effectively, which has significance for many practical medical applications. A few notable regions have been highlighted in Figures 8c and 8d.

C.3. Computational Analysis. The time taken, during the denoizing process, is an important parameter in practical medical applications. The conventional NLM is computationally expensive due to extensive number of patch comparisons. The proposed technique, conversely, is computationally efficient owing to reduced number of patch comparisons due to the robust threshold criterion and window adaptation test. We have compared the computational efficiency of different variants of the proposed algorithm with conventional NLM in terms of two parameters. First, total CPU time taken to run a particular algorithm, and second, total number of function evaluations. The most computationally expensive task, during denoizing using NLM and the proposed variants, is to compare patches for computing similarity weights. Therefore, we have used number of patch comparisons as number of function evaluations.

Figures 9a and 9b compare the CPU time and number of function evaluations, respectively, for various images used in our experiments. For each image, the results are averaged over all noise levels. Note that the IANLM-0 is not included due to its poor denoizing performance. Different variants of the proposed algorithm are implemented using the pseudo code described in Section III.B. Figure 9a shows that all the proposed variants are computationally more efficient than the conventional NLM. This computational advantage is due to the adaptive window size based on the proposed robust threshold criterion. Hence, the proposed algorithm is advantageous to the conventional NLM both in terms of CPU time and number of function evaluations.

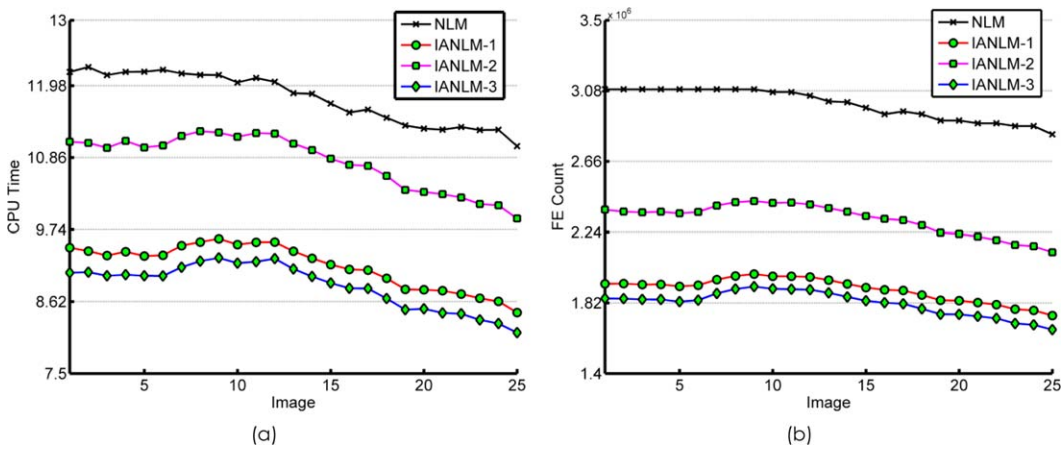

Figure 9. Computational performance of different denoizing techniques in terms of (a) CPU Time (Sec.), (b) Number of function evaluations. [Color figure can be viewed in the online issue, which is available at wileyonlinelibrary.com.]

Table V. Accuracy of Rician noise estimation using Eq. (7).

Original Noise (σ)	Estimated Noise ($\hat{\sigma}$)	Absolute Diff. (Δ)	Percentage Diff. (%)
5.00	5.0054	0.0054	0.108
10.00	10.0106	0.0106	0.106
15.00	15.0312	0.0312	0.208
20.00	20.0393	0.0393	0.197
25.00	25.0420	0.0420	0.168

D. Experiments with Real-Brain Images. The denoizing performance of the proposed IANLM algorithm is also validated for real brain MRI data. Clinical brain MR data usually suffers from problems like intensity nonuniformity, partial volume effect (PVE) and noise. The type of noise in MR imaging data is Rician, which is stronger than Gaussian noise for a particular noise level (Coupe et al., 2008). For effective results, brain MR images should be denoized prior to further computational processing. However, the amount of noise present is not known for real brain MR data and should be estimated using some noise estimation method (Sijbers et al., 1998; Nowak, 1999; Fernandez et al., 2008). A simple, yet effective, approach for Rician noise estimation is to estimate the noise from background part of square magnitude MR image (Fernandez et al., 2008). According to this method, the standard deviation of noise is computed as in the following Equation.

$$\hat{\sigma} = \sqrt{\frac{1}{2N}\sum_{k=1}^{N} M_k^2} \tag{8}$$

where M_k is the background part of the magnitude MR image, N is the number of pixels in M_k, and $\hat{\sigma}$ is the estimated noise standard deviation. The background part of the image can be obtained by any suitable threshold selection method. We have verified the effectiveness of noise estimation using Eq. (8) by estimating σ for simulated images with known noise levels. Rician noise of various levels is added to the simulated images data set and Eq. (8) is applied to estimate standard deviation for each noise level. Background part of the simulated brain images is obtained using a brain mask. The mask was created by extracting the background segment from the ground truth provided for each image in the Brainweb database. Table V shows average results of noise estimation by repeating the experiment for 50 times. It is clear from Table V that the noise estimation method used in our experiments estimates noise with great accuracy. Therefore, we estimate noise level in subsequent denoizing experiments using Eq. (8) for real brain MR data.

D.1. Performance Analysis. In this section, the donoizing performance of the proposed IANLM algorithm is compared qualitatively with conventional NLM on T_1-weighted real brain MR data. Denoizing experiments were performed in sagittal, coronal and axial views of brain MR images. The first column in Figure 10 shows original T_1-weighted brain MR images in axial, sagittal and coronal views, respectively. NLM- and IANLM-filtered images are shown in the next two columns. It can be observed that IANLM restores small structures in each image better than NLM and introduces less blurring. To observe the difference more clearly, we present residual image (difference between noisy and restored image) results in last two columns of Figure 10. The residuals are obtained for the selected portion, marked by rectangular region in the first column, and zoomed for better visualization. The proposed algorithm yields residual images which show considerably less correlation than NLM, and more structural information is visible in NLM residual images—an undesirable characteristic of residual images (Buades et al., 2005). This validates that superior quality images are produced by IANLM for all three views of T_1-weighted brain MR images.

V. APPLICATION TO SEGMENTATION

Brain MR Image segmentation is usually a subsequent stage of denoizing. Effective denoizing is indispensable for accurate segmentation. We have tested the applicability of our proposed algorithm in practical scenario of image segmentation. Brain MR Images undergo partial volume effect i.e. several tissue types may overlap in a particular voxel. Therefore, a fuzzy segmentation technique can be used effectively to segment different tissue types in brain MR images.

Fuzzy c-means (FCM) is an unsupervised clustering technique that can effectively handle such overlapping clusters (Bezdek et al., 1984). However, FCM is highly sensitive to noise present in the input image. Spatial fuzzy c-means (SFCM) (Chuang et al., 2006) resolves the problem by incorporating spatial information into FCM framework. In SFCM, cluster distribution in a certain neighborhood of a pixel is considered to alter the fuzzy membership values. This greatly reduces the effect of noise and produces more homogeneous clustering. Fuzzy local information c-means (FLICM) (Krinidis et al., 2010) incorporates more local information by introducing a fuzzy local similarity measure based on both gray level and spatial information. Besides being independent of various empirically adjusted parameters, FLICM is noise-insensitive and detail-preserving.

The fuzzy segmentation process is also greatly improved by incorporating nonlocal information into classical FCM. Fuzzy c-means with nonlocal spatial information (FCM_NLS) (Zhao et al., 2011), for example, is an extension of classical fuzzy c-means which strives to minimize a modified cost function of classical fuzzy c-means. The modified cost function incorporates nonlocal information by including a nonlocal term which operates on the NLM-restored image instead of the original one. The proposed IANLM is embedded in this segmentation framework, giving rise to fuzzy c-means with improved nonlocal spatial information (FCM_INLS). The nonlocal term in FCM_INLS operates on the image restored by IANLM instead of NLM. Therefore, FCM_INLS is able to harness the performance advantage of IANLM over NLM. The modified objective function of FCM_INLS is similar to FCM_NLS and is given as follows.

$$\mathrm{J_m} = \sum_{k=1}^{c}\sum_{i=1}^{n} u_{ki}^{m}\|y_i - v_k\|^2 + \beta\sum_{k=1}^{c}\sum_{i=1}^{n} u_{ki}^{m}\|x_i' - v_k\|^2 \tag{9}$$

where u_{ki} represents the fuzzy membership value of ith pixel for kth cluster, v_k represents the center of kth cluster, c is the total number of clusters, and n is total number of pixels in the input image. y_i represents ith pixel of the input image and m is the degree of fuzziness. The second term in Eq. (9) incorporates nonlocal information into the objective function. x_i' is the restored pixel value by IANLM filtering and β is a nonlocal tradeoff parameter that controls influence of the nonlocal term. The fuzzy membership values and cluster centroid are updated iteratively as proposed in Zhao et al. (2011).

We have applied FCM_INLS to simulated brain MR images segmentation, where ground truth segmentation is available. The simulated brain MR images are partitioned into four clusters, namely white matter (WM), gray matter (GM), cerebrospinal fluid (CSF),

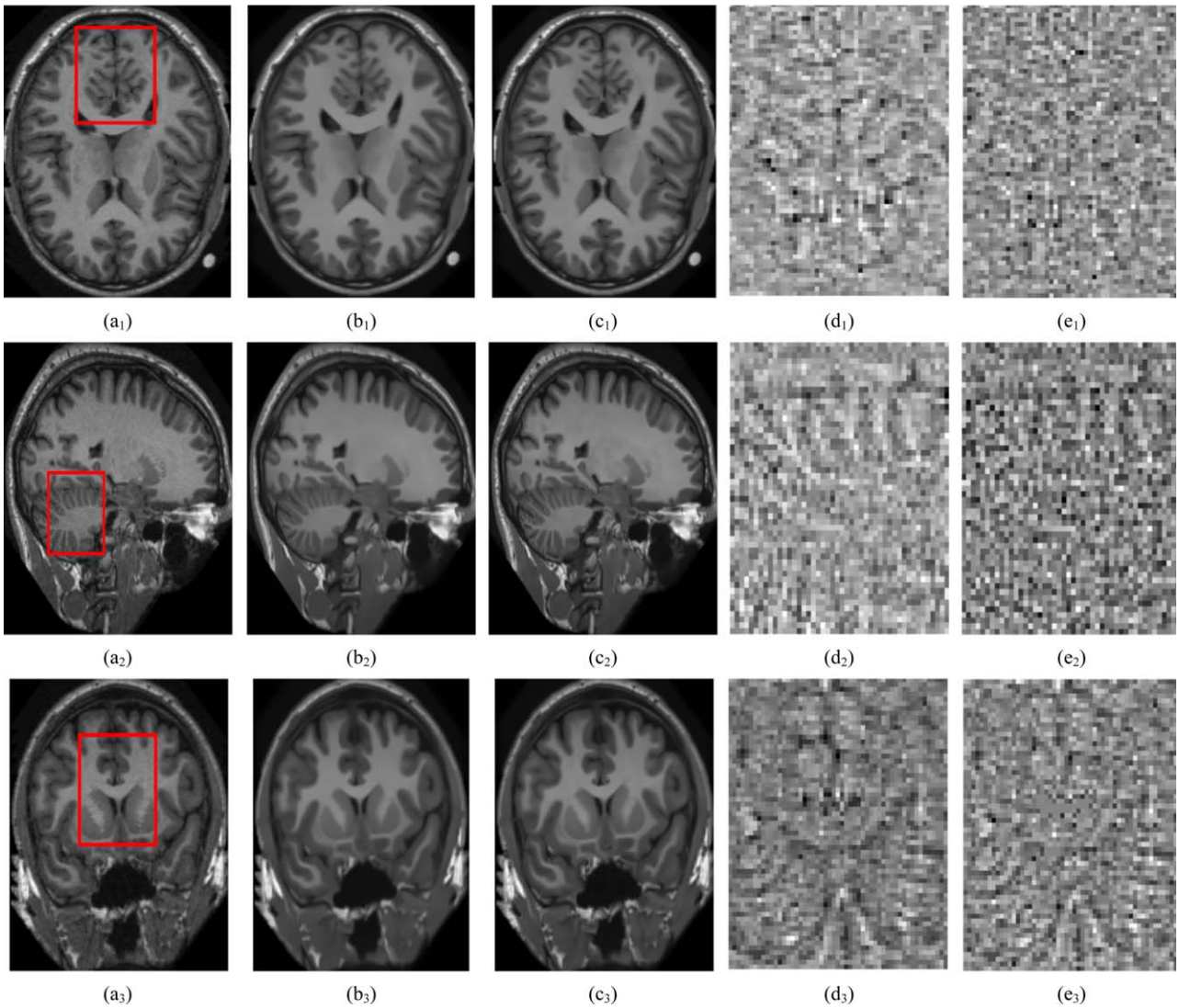

Figure 10. Qualitative results for denoizing: (a_1–a_3) real brain images in axial, sagittal and coronal views respectively, corresponding (b_1–b_3) NLM-filtered, and (c_1- c_3) IANLM-filtered images, residuals of selected portions for (d_1–d_3) NLM and (e_1–e_3) IANLM. [Color figure can be viewed in the online issue, which is available at wileyonlinelibrary.com.]

and background. The delineation of brain tissues into WM, GM and CSF has significance in many practical medical applications (Shin et al., 2009). The results of FCM_INLS have been compared with other state of the art segmentation techniques discussed previously, i.e. FCM, SFCM, FLICM and FCM_NLS.

A. Performance Metrics. The performance is measured in terms of segmentation accuracy (SA), which is a measure of overall effectiveness of the segmentation technique. It is computed as follows.

$$\mathrm{SA} = \frac{TP+TN}{\mathrm{TP+FP+TN+FN}} \times 100 \tag{10}$$

where TP, TN, FP, and FN represent true positive, true negative, false positive and false negative, respectively, obtained from confusion matrix. The confusion matrix can be easily computed by comparing segmentation result to the ground truth image.

Dice coefficient (DC) is another popular measure for evaluating the effectiveness of segmentation. It is computed, using the following equation, for two corresponding segments of the ground truth and segmented images.

$$\mathrm{DC}\,(S_i, G_i) = \frac{2|S_i \cap G_i|}{|S_i| + |G_i|}, \quad \forall i \in c \tag{11}$$

where S_i and G_i are volumes of interest in the segmented and ground truth images, respectively. Total number of clusters are represented by c in Eq. (11), whereas, $|\bullet|$serves as cardinality operator.

B. Parameter Selection. To perform brain segmentation using different segmentation techniques discussed earlier, the optimal values of various parameters involved in each segmentation technique are obtained empirically. Some of the parameters are common to all techniques, while others are unique to a particular segmentation

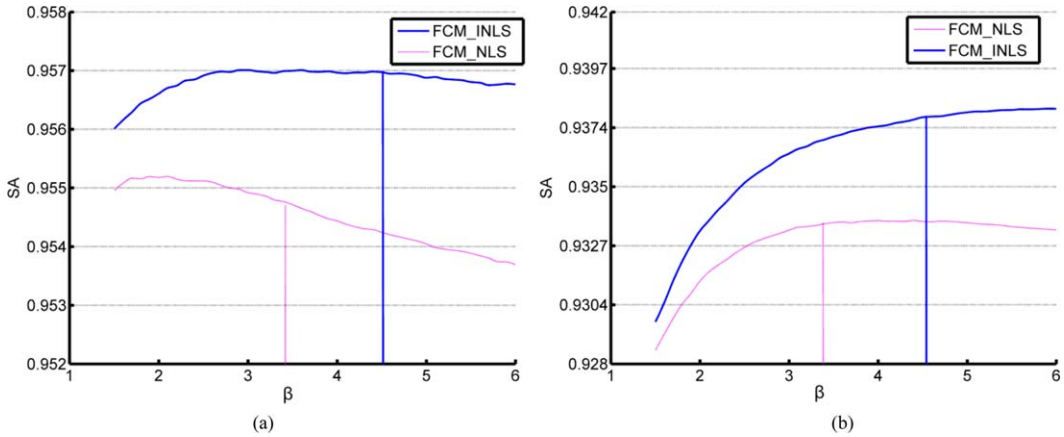

Figure 11. Selection of optimal value for beta using average segmentation accuracy on images originally corrupted with (a) 6% noise (b) 9% noise. [Color figure can be viewed in the online issue, which is available at wileyonlinelibrary.com.]

technique. The degree of fuzziness (m) and number of clusters (c), for example, are assigned the same values for all techniques, that is, 4 and 2, respectively. However, in case of SFCM and FLICM, a local window size parameter (N_{win}) is required which is empirically selected to be 5 and 3 (i.e., 5×5 and 3×3 window), respectively. The segmentation techniques FCM_NLS and FCM_INLS require images to be denoized first using NLM and IANLM, respectively. For denoizing, common parameters (s, p, and h) of NLM and IANLM and unique parameters of IANLM (N_f and w_θ) assume same values as used for simulated brain MRI denoizing in Section IV.C.

An important parameter, critical to the segmentation performance in FCM_NLS and FCM_INLS, is the nonlocal tradeoff parameter (β). The performance of each algorithm is observed over a range of prospective values of beta and, with other parameters fixed, the optimal value of beta is obtained for each algorithm. Figures 11a and 11b shows the segmentation accuracy of FCM_NLS and FCM_INLS for different values of β at two higher noise levels (6 and 9%, respectively). The vertical lines in the graphs indicate the optimal values of beta for each algorithm. Note that the value of β is different for FCM_NLS and FCM_INLS, owing to the way in which nonlocal information is exploited in NLM and IANLM. Also note that, for each algorithm, a slight performance compromise is made to obtain a single value of β, to be used for all noise levels. To summarize, Table VI reviews the optimal parameter values used in different segmentation techniques.

C. Performance Analysis. In this section, we have applied the proposed technique based FCM_INLS and other segmentation techniques to simulated brain MR images with optimal parameters (see Section V.B). The segmentation experiments are performed on NLM and IANLM-filtered images (see Section IV.C) at nine different noise levels as we did in the denoizing experiments (see Section IV.C). The segmentation performance is measured in terms of segmentation accuracy (SA). For each noise level, the results are averaged over all the slices and reported in Table VII. The quantitative results in Table VII show that FCM_INLS has successfully segmented the brain MR images into desired number of clusters while maintaining higher SA at all noise levels.

In addition to overall segmentation accuracy, we have also computed DC for each tissue type in brain MR images. This helps to determine the effectiveness of delineating each tissue type separately, which is useful in certain medical applications (Shin et al., 2009). Figure 12 graphically compares DC values for WM, GM and CSF, obtained using different segmentation techniques. For all tissue types, the proposed technique based FCM_INLS outperforms other techniques at almost all noise levels (specially for the CSF case). Other techniques such as FCM and FLICM show an exponential decay in performance as noise level increases; however, the proposed FCM_INLS exhibits graceful degradation (linear behavior). Therefore, it can be speculated that FCM_INLS will also perform better at higher noise levels as compared to other techniques.

Finally, we present visual results of segmentation achieved by using our proposed scheme based FCM_INLS and other segmentation techniques. Figures 13a, 13b, and 13c, respectively, show a particular simulated brain MR image, from the 3D brain volume, along with corresponding noisy images corrupted by 5 and 9% Rician

Table VI. Optimal parameter values for different segmentation techniques.

Segmentation Algorithm	Parameters						
	c	m	N_{win}	S	p	h	B
FCM	4	2	–	–	–	–	–
SFCM	4	2	5	–	–	–	–
FLICM	4	2	3	–	–	–	–
FCM_NLS	4	2	–	5	2	1.2σ	3.3
FCM_INLS	4	2	–	5	2	1.2σ	4.5

Table VII. Simulated brain MRI segmentation accuracy of different techniques at various noise levels.

Noise (%)	Segmentation Accuracy				
	FCM	SFCM	FLICM	FCM_NLS	FCM_INLS
1	98.70	97.23	98.24	98.34	98.66
2	97.87	95.12	97.19	97.51	97.92
3	97.10	94.99	96.79	97.12	97.38
4	96.14	94.82	96.29	96.63	96.87
5	94.86	94.60	95.64	96.06	96.29
6	93.08	94.34	94.80	95.43	95.67
7	90.96	94.05	93.82	94.81	95.08
8	88.14	93.71	92.48	94.08	94.40
9	84.56	93.26	90.83	93.30	93.71

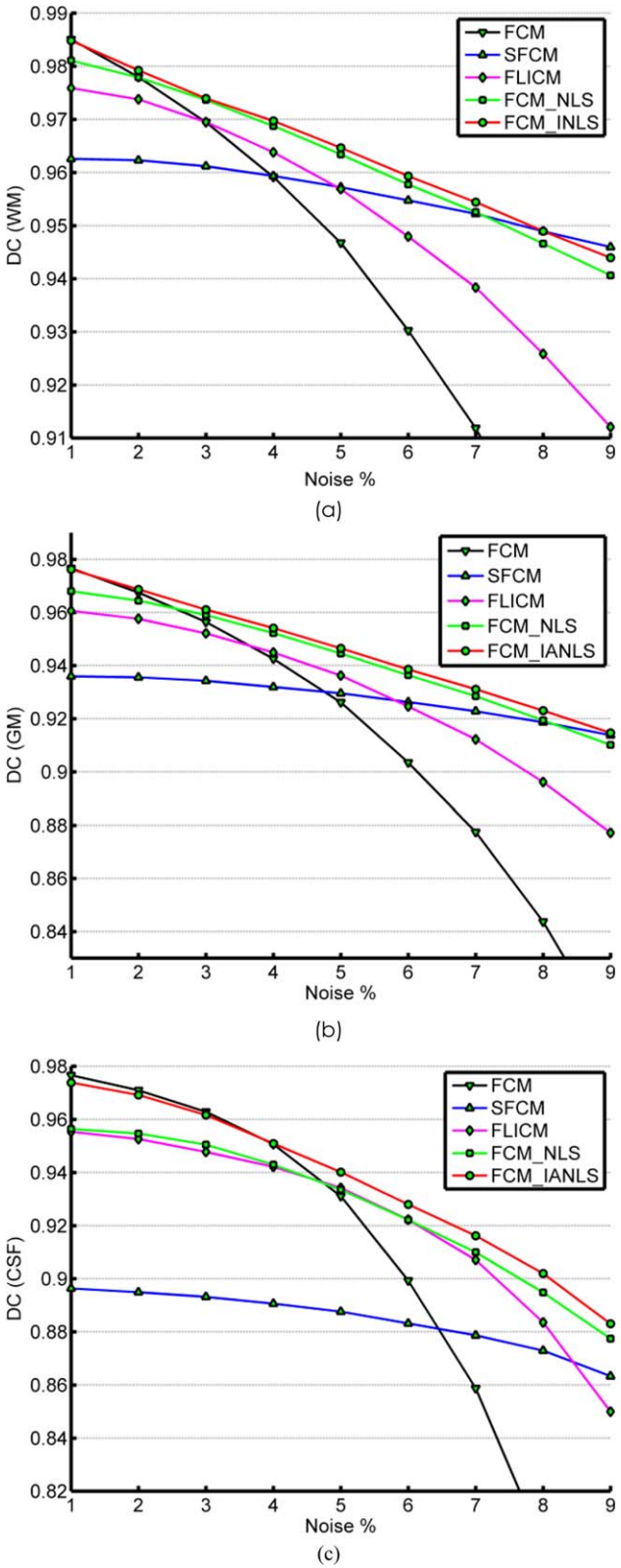

Figure 12. Dice Coefficient values using different segmentation techniques for, (a) white matter (WM), (b) gray matter (GM), and (c) cerebrospinal fluid (CSF). [Color figure can be viewed in the online issue, which is available at wileyonlinelibrary.com.]

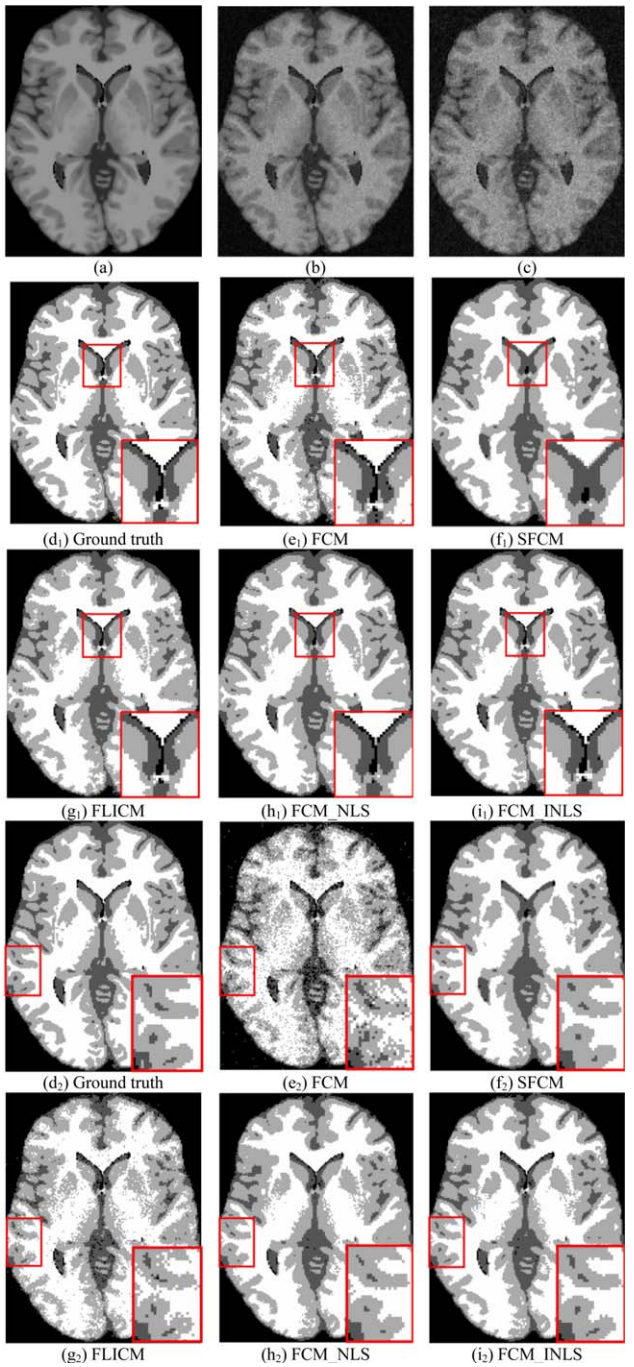

Figure 13. Segmentation results using different segmentation techniques (a) original image, original image corrupted with (b) 5% noise, and (c) 9% noise, (d_1,d_2) ground truth segmentation, visual segmentations for (e_1–i_1) noise = 5%, and (e_2–i_2) noise = 9%. [Color figure can be viewed in the online issue, which is available at wileyonlinelibrary.com.]

noise. The ground truth segmentation and segmented images produced by different techniques are shown in Figure 13 (d_1–i_1) and (d_2–i_2), for 5 and 9% noise, respectively. Visual results verify better segmentation results produced by FCM_INLS as compared to other segmentation techniques. For better view, a rectangular portion is zoomed in each image where the difference can be realized more clearly. It is clear that FCM and FLICM are sensitive to higher levels

of noise, while SFCM results in over-segmentation at various points in the image. Similarly, FCM_INLS produces better results than FCM_NLS as evident from the zoomed portions in Figure 13 (h_1, i_1) and (h_2, i_2). Hence, overall, the segmentation produced by FCM_INLS is much closer to the ground truth.

VI. CONCLUSION

Nonlocal means is a classical denoizing technique of effective image restoration being used in many practical application. The restoration process is based on similarity weights computed from image patches. In this research, we have proposed a novel variant of NLM by introducing two complementary modifications. First, a robust threshold criterion is introduced, which helps selecting suitable pixels for participation in the restoration process. Second, the window size is made adaptive based on a window adaptation test. Hence, the proposed variant is named as improved adaptive nonlocal means (IANLM). To better exploit local information in the proposed scheme, an alternate implementation of IANLM is proposed. The validation of the proposed scheme is performed by denoizing synthetic and real brain MR data. After denoizing synthetic brain images, performance results, in terms of PSNR, RMSE and correlation, and computational measures, in terms of CPU time and number of function evaluations, are obtained for classical NLM and different IANLM-based denoizing schemes. The results verify that IANLM not only performs denoizing more effectively, but is also computationally efficient. Real clinical brain MR images are also denoized using NLM and IANLM. Qualitative comparison of denoized images and corresponding residuals verify superiority of IANLM for real images as well. Finally, the proposed scheme is also incorporated into a segmentation framework to verify its practical applicability. The segmentation performance is compared in terms of segmentation accuracy and DICE coefficient. The proposed scheme-based segmentation technique outperformed all other techniques. Hence, the proposed algorithm can be used reliably in practical medical applications.

ACKNOWLEDGMENTS

The authors like to express their appreciation for McConnell Brain Imaging Center (BIC) of the Montreal Neurological Institute, for publicly sharing the simulated brain MR data (http://www.bic.mni.mcgill.ca/brain-web). They also like to acknowledge Randy Buckner, Daniel Marcus, and Washington University Alzheimer's Disease Research Center for sharing Open Access Series of Imaging Studies (OASIS, www.oasis-brains.org) real brain MRI database.

REFERENCES

M. Aksam, S. Rathore, and A. jalil, Parameter Optimization for Non-Local De-noising using Elite GA, International Multitopic Conference, Islamabad, Pakistan, 2012.

I. Bankman, Handbook of medical imaging: Processing and analysis, Academic Press, New York, 2000.

J.C. Bezdek, R. Ehrlich, and W. Full, FCM: The Fuzzy C-Means clustering algorithm, Comput Geosci 10 (1984), 191–203.

A. Buades, B. Coll, and J.M. Morel, A review of image denoising algorithms with a new one, Multiscale Model Simul 4 (2005), 490–530.

K.S. Chuang, H.L. Tzeng, S. Chen, J. Wu, and T.J. Chen, Fuzzy c-means clustering with spatial information for image segmentation, Comput Med Imaging Graphics 30 (2006), 9–15.

D.L. Collins, A.P. Zijdenbos, V. Kollokian, J.G. Sled, N.J. Kabani, C.J. Holmes, and A.C. Evans, Design and construction of a realistic digital brain phantom, IEEE Trans Med Imaging 17 (1998), 463–468.

P. Coupe, P. Yger, S. Prima, P. Hellier, C. Kervrann, and C. Barillot, An optimized blockwise nonlocal means denoising filter for 3-D magnetic resonance images, IEEE Trans Med Imaging 27 (2008), 425–441.

J. Feng, L.C. Jiao, X. Zhang, M. Gong, and T. Sun, Robust non-local fuzzy c-means algorithm with edge preservation for SAR image segmentation, Signal Process 93 (2013), 487–499.

S.A. Fernandez, C.A. Lopez, and C.F. Westin, Noise and signal estimation in magnitude MRI and Rician distributed images: A LMMSE approach, IEEE Trans Image Process 17 (2008), 1383–1398.

Y. Gal, A.J.H. Mehnert, A.P. Bradley, K. McMahon, D. Kennedy, and S. Crozier, Denoising of dynamic contrast-enhanced mr images using dynamic nonlocal means, IEEE Trans Med Imaging 29 (2010), 302–310.

G. Gerig, O. Kübler, R. Kikinis, and F. Jolesz, Nonlinear anisotropic fitering of MRI data, IEEE Trans Med Imaging 11 (1992), 221–232.

H. Gudbjartsson and S. Patz, The rician distribution of noisy MRI data, Magn Reson Med 34 (1995), 910–914.

M. Hassan, A. Chaudhr, A. Khan, and J.Y. Kim, Carotid artery image segmentation using modified spatial fuzzy c-means and ensemble clustering, Comput Methods Prog Biomed 108 (2012), 1261–1276.

Z. Ji, Y. Xia, Q. Chen, Q. Sun, D. Xia, and D.D. Feng, Fuzzy c-means clustering with weighted image patch for image segmentation, Appl Soft Comput 12 (2012), 1659–1667.

S. Krinidis and V. Chatzis, A robust fuzzy local information C-means clustering algorithm, IEEE Trans Image Process 19 (2010), 1328–1337.

R.K.S. Kwan, A.C. Evans, and G.B. Pike, An Extensible MRI Simulator for Post-Processing Evaluation, Visualization in Biomedical Computing, Lecture Notes in Computer Science, Springer-Verlag, Hamburg, Germamy, 1996, pp. 135–140.

M.J. Kwon, Y.J. Han, I.H. Shin, and H.W. Park, Hierarchical fuzzy segmentation of brain MR images, Int J Imaging Syst Technol 13 (2003), 115–125.

Y.L. Liu, J. Wang, X. Chen, Y.W. Guo, Q.S. Peng, A robust and fast nonlocal means algorithm for image denoising, J Comput Sci Technol 23 (2008), 270–279.

A. Macovski, Noise in MRI, Magn Reson Med 36 (1996), 494–497.

J.V. Manjon, J.C. Caballero, J.J. Lull, G.G. Marti, L.M. Bonmati, and M. Robles, MRI denoising using non-local means, Med Image Anal 12 (2008), 514–523.

J.V. Manjon, P. Coupe, L.M. Bonmatí, D.L. Collins, and M. Robles, Adaptive non-local means denoising of mr images with spatially varying noise levels, J Magen Reson Imaging 31 (2010), 192–203.

D.S. Marcus, T.H. Wang, J. Parker, J.G. Csernansky, J.C. Morris, and R.L. Buckner, Open access series of imaging studies (OASIS): Cross-sectional MRI data in young, middle aged, nondemented, and demented older adults, J Cogn Neurosci 19 (2007), 1498–1507.

R.D. Nowak, Wavelet-based rician noise removal for magnetic resonance imaging, IEEE Trans on Image Process 8 (1999), 1408–1419.

E. Ordentlich, G. Seroussi, S. Verdu, M. Weinberger, T. Weissman, A discrete universal denoiser and its application to binary images, IEEE International Conference on Image Processing, Barcelona, Spain, 2003, pp. 117–120.

S. Saha and U. Maulik, A new line symmetry distance based automatic clustering technique: Application to image segmentation, Int J Imaging Syst Technol 21 (2011), 86–100.

J. Salmon, On two parameters for denoising with Non-Local Means, Signal Process Lett 17 (2010), 269–272.

J. Sijbers, A.J.D. Dekker, D.V. Dyck, and E. Raman, Estimation of signal and noise from Rician distributed data, Proceedings of the International Conference on Signal Processing and Communications, Gran Canaria, Spain, 1998, 140–142.

W. Shin, G. Xiujuan, H. Gu, and Y. Yang, Brain Tissue Segmentation using Fast T1 Mapping, Proceedings of the International Society for Magnetic Resonance in Medicine, Honolulu, Hawaii, 2009.

T. Thaipanich and C.C.J. Kuo, An Adaptive Nonlocal Means Scheme for Medical Image Denoising, Proceedings of SPIE., Medical Imaging, San Diego, California, 2010.

A.T. Vega, V.G. Perez, S.A. Fernandez, and C.F. Westin, Efficient and robust nonlocal means denoising of MR data based on salient features matching, Comput Methods Prog Biomed 105 (2012), 131–144.

R. Yan, L. Shao, S.D. Cvetkovic, and J. Klijn, Improved nonlocal means based on pre-classification and invariant block matching, J Display Technol 8 (2012), 212–218.

L. Yaroslavsky, Digital picture processing, an introduction, Springer-Verlag, Berlin, 1985.

F. Zhao, L. Jiao, and H. Liu, Fuzzy c-means clustering with non local spatial information for noisy image segmentation, Front Comput Sci China 5 (2011), 45–56.